Electronic Supplementary Material (ESI) for New Journal of Chemistry.

SUPPLEMENTARY MATERIAL

Magnetic amphiphilic nanocomposites based on silica/carbon for diesel desulfurization

Aline A. S. Oliveira[a], Taís Christofani[a], Ivo F. Teixeira[b], José D. Ardisson[c], Flávia C. C. Moura[a*]

a Departamento de Química, ICEx, Universidade Federal de Minas Gerais, Av. Antônio Carlos 6627, Belo Horizonte, Brazil. Fax: 55 31 34095700, Tel: 55 31 34097556. flaviamoura@ufmg.br

b Department of Chemistry, University of Oxford, OX1 3QR, UK.

c Laboratório de Física Aplicada, CDTN. Belo Horizonte, MG, Brazil.

The temperature-programmed reactions used in the synthesis of amphiphilic materials were studied. The technique of temperature programmed reduction (TPR) is part of a diverse set of techniques for temperature-programmed reactions applied in general to study the activation and reactivity of heterogeneous catalysts.

The technique consists of monitoring the reduction of a sample exposed to a continuous flow of H_2 and heated in a linear temperature ramp. H_2 consumption is monitored and the appearance of a positive signal in a TPR analysis indicate the consumption of H_2 by the sample.

The novelty in the synthesis of the amphiphilic materials is the TPCVD technique, inspired by the TPR. The technique TPCVD consists in the study of a CVD (chemical vapor deposition) reaction at temperature-programmed. It uses the same system of the TPR, but the sample is heated under a gas flow of carbon source, in this case CH_4. The

* Corresponding author: Tel.: +55 31 3409 5719; Fax.: +55 31 3409 5777. E-mail address: flaviacrismoura@gmail.com

decomposition of methane to carbon deposits on the surface of the material generates H_2, which is detected by TCD detector. But unlike the TPR analysis the generated signal is negative, indicating H_2 production. This signal can be directly related to the amount of carbon deposited on the sample.

The registers of **Figure S1(a)** refer to hydrogen consumption as the temperature rise with the reduction of metallic ions (TPR experiment). As the records of **Figure S1(b)** refer to hydrogen production by increasing the temperature for carbon deposition (TPCVD experiment).

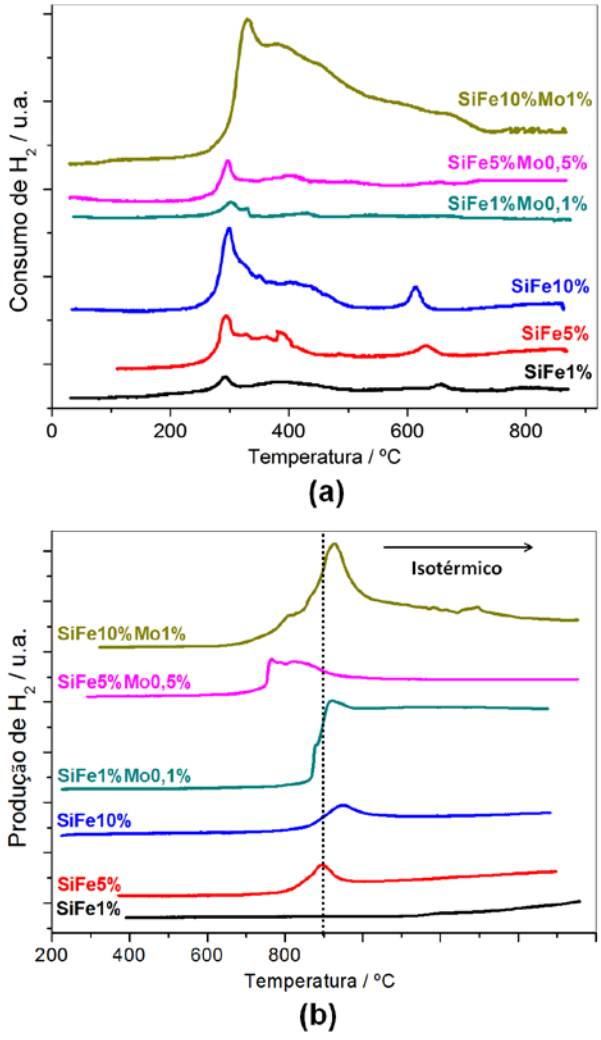

Figure S1. (a) TPR and (b) TPCVD profiles obtained.

The TPR profiles (**Figure S1(a)**) obtained for silica impregnated with different concentrations of iron in the absence of molybdenum showed peaks characteristic of the reduction of iron phases: reduction of Fe^{3+} to Fe^{2+} between 300 and 400 ^{o}C and a reduction of Fe^{2+} to Fe^{0} between 600 and 700 ^{o}C. In the presence of molybdenum, reduction peaks suffer position and intensity changes, suggesting that an interaction occurs between metals supported, possibly forming an alloy between Fe and Mo and also an interaction between Fe and SiO_2, such as in the form of $FeSiO_4$.

The metallic sites of iron and molybdenum catalyze the decomposition of methane, depositing solid carbon on the surface of the materials and releasing hydrogen gas, which is detected and generates TPCVD signal (**Figure S1(b)**). Therefore, the area above the TPCVD curves is proportional to the amount of carbon deposited on the materials. In the TPCVD profiles obtained there is an asymmetric peak. The more symmetrical peak generated, the more organized carbon deposited. Therefore, the materials and SiFe5% and SiFe10%Mo1% are those which should contain a higher concentration of carbon filaments.

Table S1. Hyperfine parameters obtained by Mössbauer spectroscopy for the amphiphilic materials.

Sample	Phase	δ / mm s^{-1} (± 0.05)	ε,Δ / mm s^{-1} (± 0.05)	B_{hf} / T (± 0.2)	RA / % (± 1)
SiFe5%	γ-Fe(C)	-0.10	-	-	38
	Fe^{2+}	1.18	2.805	-	34
	Fe^{2+}	1.68	1.75	-	28
SiFe5%Mo0.5%	Mix Fe_xC_y (X = 3,5,7 e Y = 1,3,5)	0.19 0.15	0 0	23.6 19.3	16 51
	γ-Fe(C)	-0.10	-	-	12
	Fe^{3+}	0.18	0.62	-	21
SiFe10%	γ-Fe(C)	-0.15	-	-	50
	Fe^{2+}	1.23	2.59	-	39
	Fe^{2+}	1.65	1.75	-	11
SiFe10%Mo1%	Fe^0	0.00	0.00	33.0	20
	Fe_xC_y (X = 3,5,7 e Y = 1,3,5)	0.15	0	19.7	55
	γ-Fe(C)	-0.20	-	-	13
	Fe^{3+}	0.33	0.60	-	12

δ – relative isomeric shift relative to α-Fe; ε – quadrupole shift; Δ – quadrupole splitting; B_{hf} – hyperfine magnetic field; RA – relative subspectral area.

Figure S2 shows the patterns of X-ray diffraction obtained for each material.

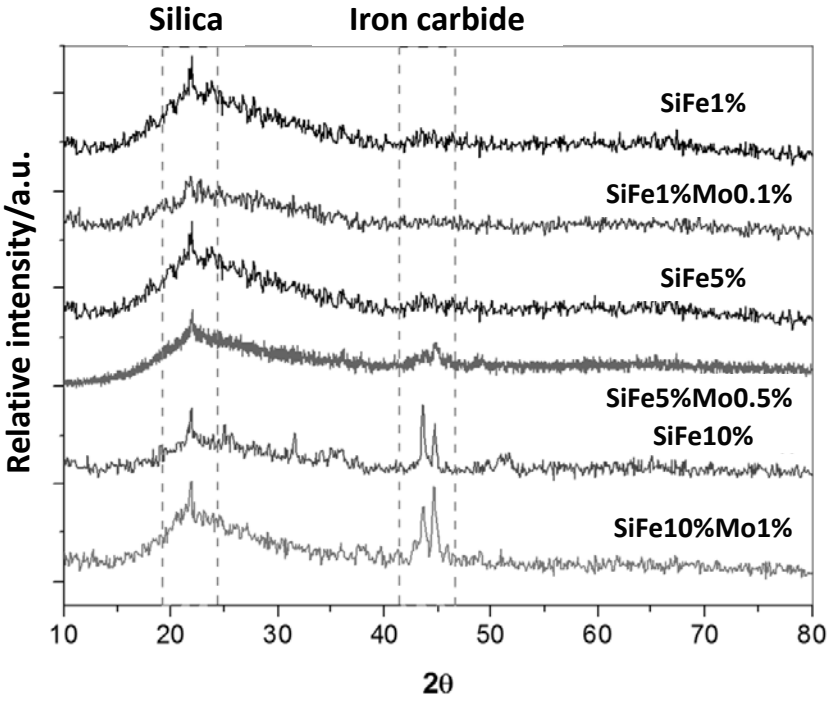

Figure S2. X-ray diffraction patterns obtained for the amphiphilic materials.

The amphiphilic magnetic materials synthesized underwent thermo analysis (TG) under synthetic air flow (**Figure S3**). In detail is shown the carbon content of the materials obtained by elemental analysis.

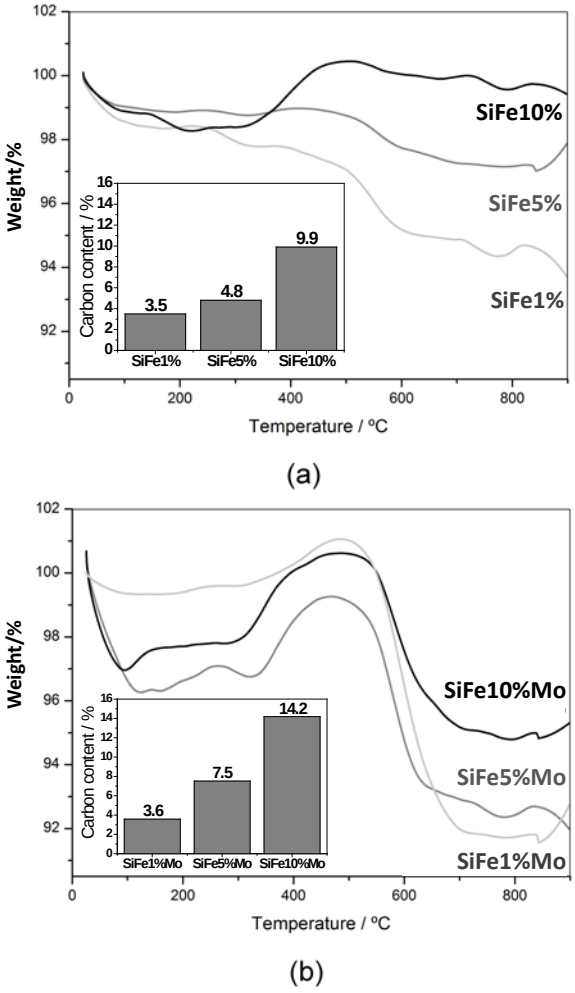

Figure S3. TG curves of the materials: (a) without Mo and (b) with Mo, obtained under air flow and elemental analysis results in detail.

Table S2. Carbon content obtained by CHN elemental analysis

Sample	C / %
SiFe1%	3.5
SiFe5%	4.8
SiFe10%	9.9
SiFe1%Mo0.1%	3.6
SiFe5%Mo0.5%	7.5
SiFe10%Mo1%.	14.2

TG curves of **Figure S3** obtained for the materials show a weight gain in the temperature range between 350 and 550 ^{o}C. This gain can be related to the oxidation of reduced iron phases to Fe_2O_3 and reduced molybdenum phases to MoO_3 (**Equations S1 and S2).** As expected, the larger the amount of iron and molybdenum, the greater the weight gain.

$2Fe^0(s) + 3/2\ O_2(g) \rightarrow Fe_2O_3(s)$ (**Equation S1**)

$Mo^0(s) + 3/2\ O_2(g) \rightarrow MoO_3(s)$ (**Equation S2**)

The weight gain shown in the curves of materials containing molybdenum is more significant than for those containing only iron. This difference is mainly due to two factors: (i) combination of events, oxidation of iron and molybdenum at the same time and (ii) proportion metal:oxygen. The iron oxide formed is composed of 2Fe:3O and the molybdenum oxide of 1Mo:3O, which means that more oxygen is consumed in the formation of MoO_3.

Also for the TG curves obtained for the materials, there are two events of weight loss. The first of them from room temperature to 200 ^{o}C and the second after 500 ^{o}C. The first weight loss can be associated essentially with loss of water. Carbon is oxidized at higher temperatures, leading to the second event of weight loss up to 500 ^{o}C ($C_{(s)} + O_{2(g)} \rightarrow CO_{2(g)}$). Materials which have molybdenum in the composition should have a higher content of carbon as their weight loss at higher temperatures are more expressive [1].

It is important to note that the oxidation events described separately may overlap throughout the analysis. Therefore, the thermal analysis applied to this set of samples provides only semi-quantitative information on the composition of materials.

Figure S4 shows the performance of the amphiphilic magnetic materials in the formation and breaking of emulsions.

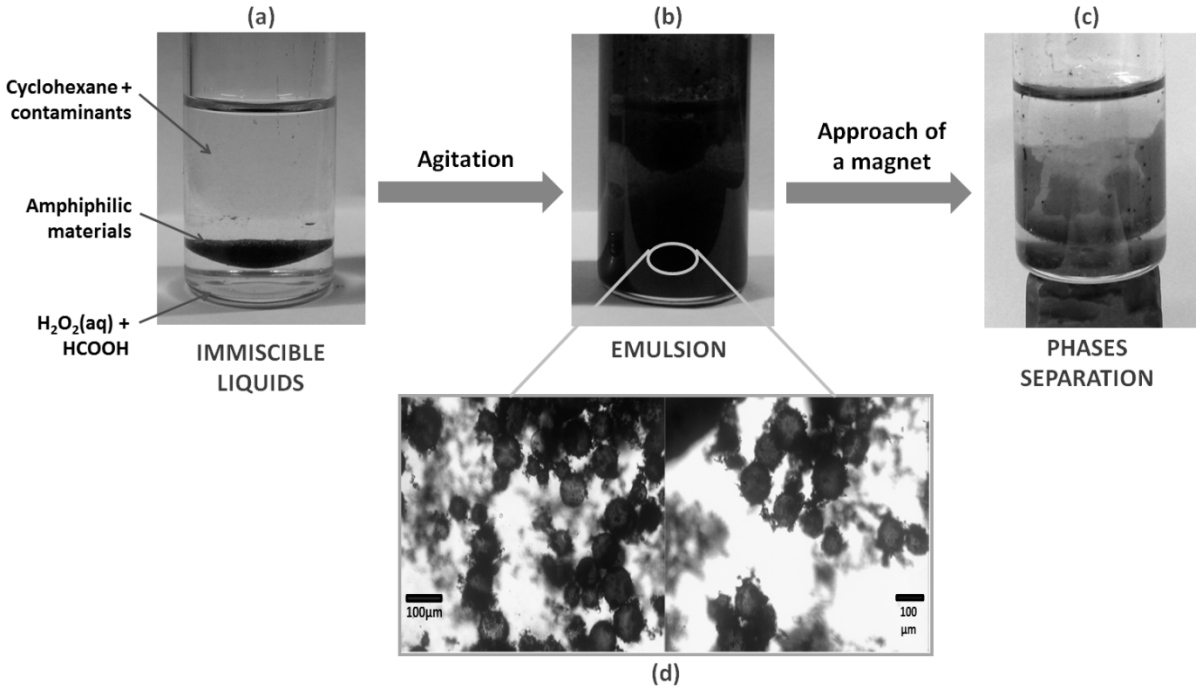

Figure S4. Performance of materials in the formation and breaking of emulsion.

Figure S4(a) shows the biphasic system after addition of amphiphilic material, but before stirring. The preferred position of the materials between the two phases depends on their amphiphilicity. It was observed that the materials with greater hydrophilic character (less carbon) are preferably located in the aqueous phase, while the hydrophobic materials (higher carbon content) tend to migrate into the oil phase. After stirring, a stable emulsion is formed (**Figure S4(b)**) with materials particles around the oil droplets dispersed in water. The emulsion was characterized by optical microscopy (**Figure S4(d)**). With the approach of a magnetic field, the materials are drawn by

promoting the separation of the phases (**Figure S4(c)**).

The probable mechanism for biphasic catalytic oxidation promoted by amphiphilic materials produced is sketched in **Figure S5**.

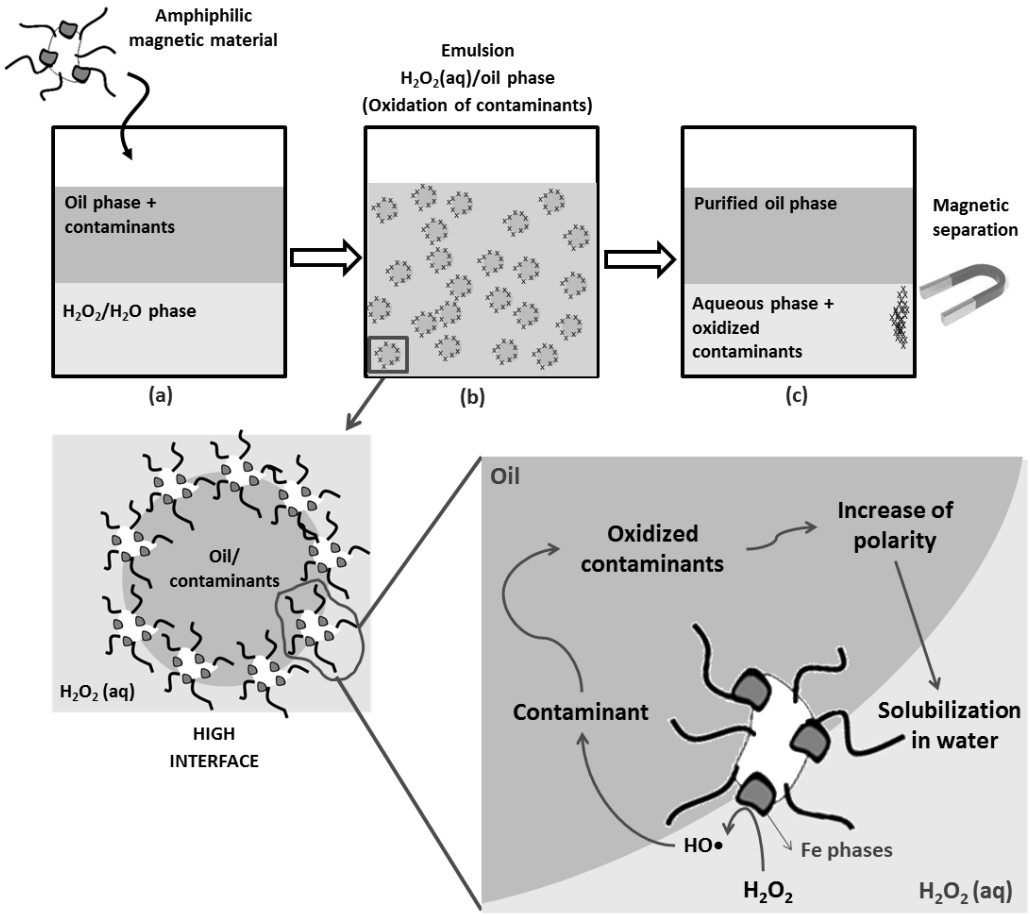

Figure S5. Probable mechanism of a biphasic oxidation of organic contaminants in the presence of the amphiphilic materials.

It is observed in the reaction mechanism (**Figure S5**) that the amphiphilic magnetic materials play a dual role in the oxidation reaction. First, they act as a solid emulsifiers promoting the stabilization of an oil/water emulsion and hence a higher interface

between the immiscible phases. Second, they catalyze the heterogeneous Fenton like reaction by decomposition of hydrogen peroxide, which generates hydroxyl radicals (•OH): extremely strong oxidants, capable of oxidizing a wide range of organic contaminants.

At the end of reaction, the amphiphilic magnetic materials are still responsible for the promotion of phase separation. Via approaching of an external magnetic field, the particles are easily removed from the interface destabilizing the emulsion.

It can also be seen in Figure S5 that the oxidation products thus more polar than their precursors are solubilized and extracted by the aqueous phase.

In order to investigate the reaction kinetics with each of the catalysts, the reactions were considered as pseudo first order reactions depending mainly on the concentration of the contaminant, since the oxidizer is in excess and its concentration varies very little throughout the reaction. Thus, the rate law for this reaction can be expressed as **Equation S3**:

$$\frac{-\mathrm{d}[\mathrm{DBT}]}{\mathrm{dt}} = \mathrm{k}\,[\mathrm{DBT}] \qquad \textbf{(Equation S3)}$$

Equation S3 can be rewritten as follows:

$$\frac{\mathrm{d}[\mathrm{DBT}]}{\mathrm{dt}} = -\,\mathrm{k}\,[\mathrm{DBT}]$$

Integrating the concentration of DBT between the initial concentration $[DBT]_0$ and the concentration at time t [DBT] (**Equation S4**), we obtain **Equation S5**:

$$\int_0^{\mathrm{t}} \frac{\mathrm{d}[\mathrm{DBT}]}{[\mathrm{DBT}]} = -\int_0^{\mathrm{t}} \mathrm{k}\,\mathrm{dt} \qquad \textbf{(Equation S4)}$$

$$\ln \frac{[\mathrm{DBT}]}{[\mathrm{DBT}]_0} = -\mathrm{kt} \qquad \textbf{(Equation S5)}$$

Thus, the linearization of the curves was done as shown in **Figure S6**.

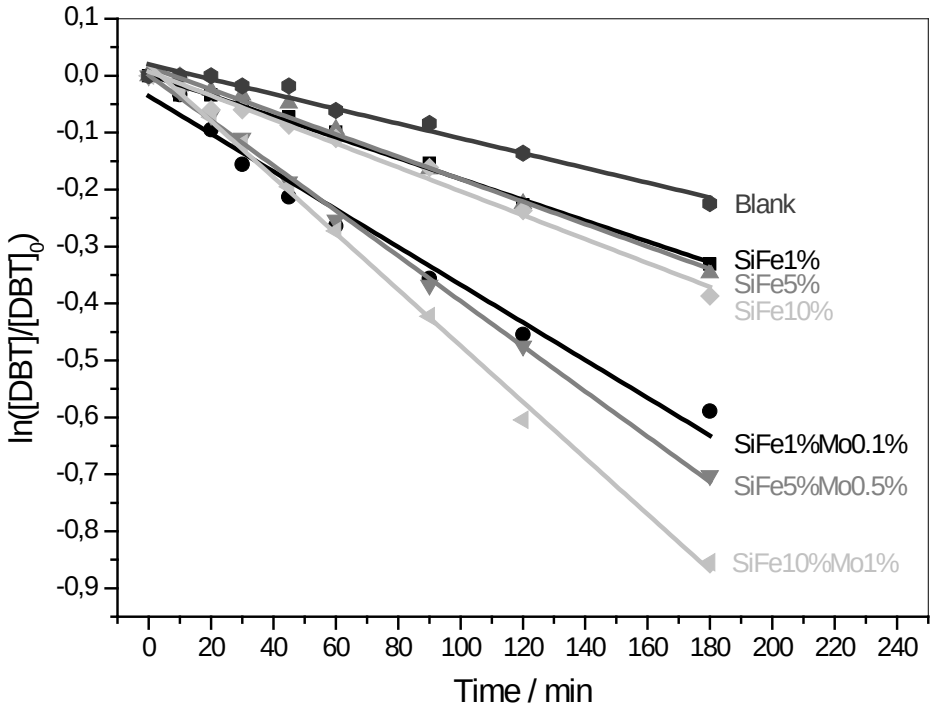

Figure S6. Kinetics of DBT removal in the presence of the materials.

Reaction rate were obtained for the experiments in the presence of each material and also for the blank (**Figure S7**). The value of the reaction rate was determined by the slope of the lines generated.

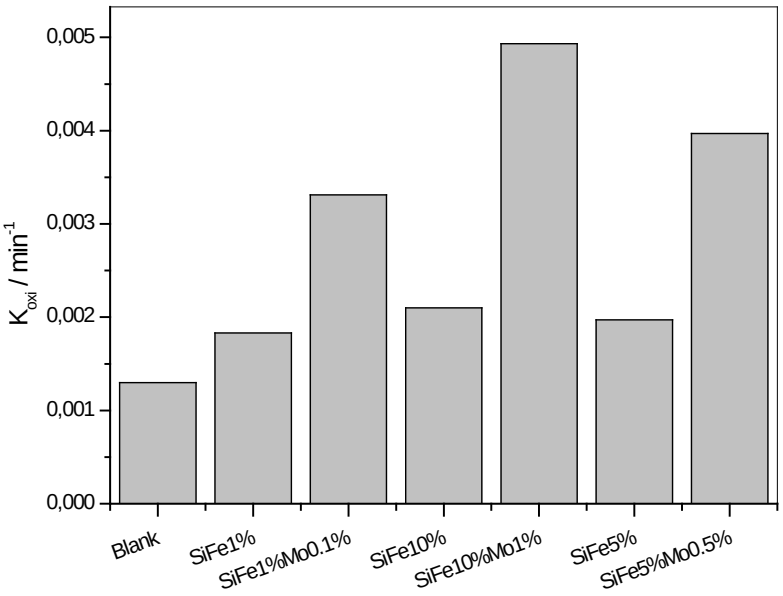

Figure S7. Reaction rate for DBT oxidation.

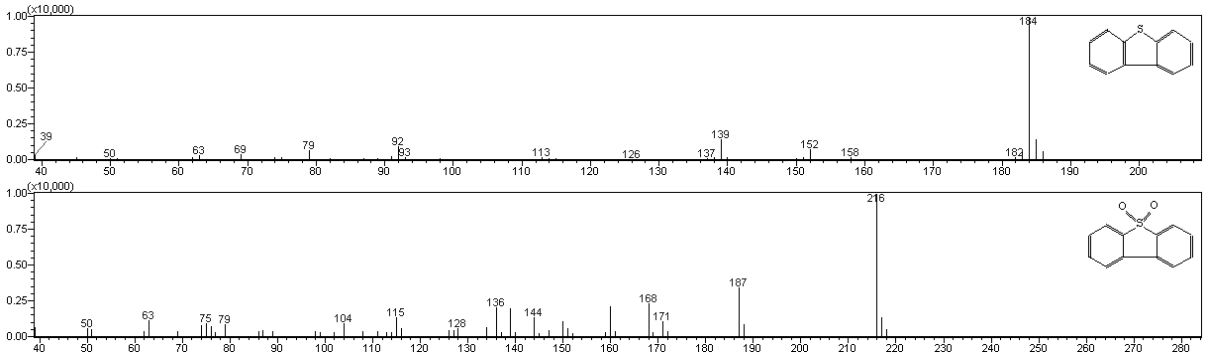

Figure S8. Mass spectra obtained for peaks 1 and 2 of the chromatogram, respectively.

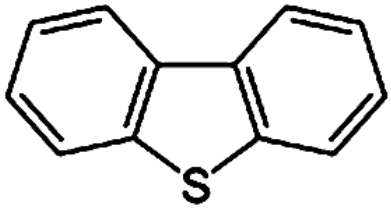

Figure S9. Structure of dibenzothiophene used as model organic sulfur contaminant in the oxidation tests.

Experiments with colored phases showed that oil-in-water emulsions are formed in the presence of the composites (**Figure S10(a)**). Materials on the interface of cyclohexane droplets dispersed in water were analyzed by Raman spectroscopy. In **Figure S10(b)** is shown an expansion of the regions on the droplet surface that were analyzed and **Figure S10(c)** shows average Raman spectra obtained for these regions.

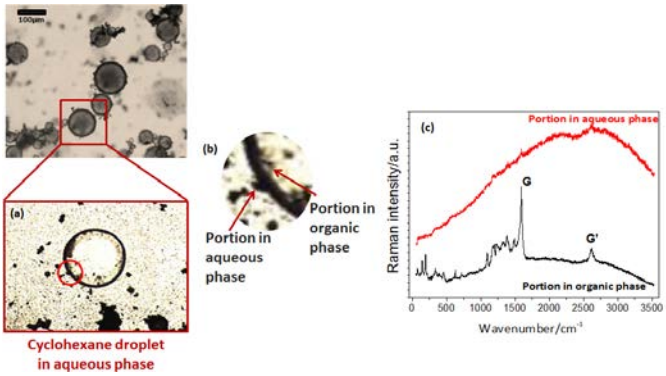

Figure S10. Orientation of silica/carbon composites in emulsions, obtained by Raman spectroscopy.

Raman spectrum obtained for the portion of the composite inside the organic droplet presents intense bands characteristic of C nanostructures, i.e. G and G' bands around

1580 and 2600 cm^{-1}, respectively. This indicates that the carbon structures are directed towards the nonpolar part of the system. On the other hand, spectrum obtained for the portion of the material in the aqueous phase does not show any peaks that could be associated with carbon organization, indicating that this portion could be formed mainly by silica with Fe/Mo. It is known that the pattern in which emulsifiers adsorb on the interface is well defined, due to the affinity of different parts of the material by aqueous or oil phases. Hydrophilic ends should be aligned with aqueous phase; while lipophilic aligned with oil phase, forming an oriented and stable film[49]. Crossley *et al.* have shown the same organization of similar materials by transmission electron microscopy[50]. **Figure S11** shows the proposed mechanism of desulfurization in the presence of the magnetic amphiphilic silica/carbon composites.

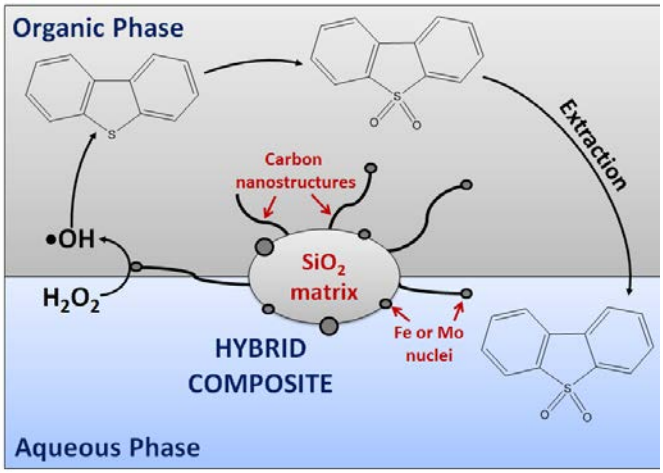

Figure S11. Mechanism of desulfurization catalyzed by the amphiphilic composites.

[1] A.A.S. Oliveira, I.F. Teixeira, L.P. Ribeiro, E. Lorençon, J.D. Ardisson, L. Fernandez-Outon, W.A.A. Macedo, F.C.C. Moura, Applied Catalysis A: General 456 (2013) 126-134.
[2] R. Gerber, in: e.G.A.D. Kluwer) (Ed.), 1994, pp. 165–220.